Medical Engineering & Physics 36 (2014) 1305–1311

Contents lists available at ScienceDirect

Medical Engineering & Physics

journal homepage: www.elsevier.com/locate/medengphy

Representation of fluctuation features in pathological knee joint vibroarthrographic signals using kernel density modeling method

Shanshan Yang [a], Suxian Cai [a], Fang Zheng [a], Yunfeng Wu [a,*], Kaizhi Liu [a], Meihong Wu [a], Quan Zou [a], Jian Chen [b]

[a] School of Information Science and Technology, Xiamen University, Xiamen, Fujian, China
[b] Department of Rehabilitation, Zhongshan Hospital, Xiamen University, Xiamen, Fujian, China

ARTICLE INFO

Article history:
Received 27 June 2013
Received in revised form 1 March 2014
Accepted 8 July 2014

Keywords:
Knee joint
Vibroarthrography
Signal processing
Envelope
Detrended fluctuation analysis
Kernel density estimation
Bayesian decision rule
Support vector machine

ABSTRACT

This article applies advanced signal processing and computational methods to study the subtle fluctuations in knee joint vibroarthrographic (VAG) signals. Two new features are extracted to characterize the fluctuations of VAG signals. The fractal scaling index parameter is computed using the detrended fluctuation analysis algorithm to describe the fluctuations associated with intrinsic correlations in the VAG signal. The averaged envelope amplitude feature measures the difference between the upper and lower envelopes averaged over an entire VAG signal. Statistical analysis with the Kolmogorov–Smirnov test indicates that both of the fractal scaling index ($p = 0.0001$) and averaged envelope amplitude ($p = 0.0001$) features are significantly different between the normal and pathological signal groups. The bivariate Gaussian kernels are utilized for modeling the densities of normal and pathological signals in the two-dimensional feature space. Based on the feature densities estimated, the Bayesian decision rule makes better signal classifications than the least-squares support vector machine, with the overall classification accuracy of 88% and the area of 0.957 under the receiver operating characteristic (ROC) curve. Such VAG signal classification results are better than those reported in the state-of-the-art literature. The fluctuation features of VAG signals developed in the present study can provide useful information on the pathological conditions of degenerative knee joints. Classification results demonstrate the effectiveness of the kernel feature density modeling method for computer-aided VAG signal analysis.

1. Introduction

The knee joint is an intricate synovial joint that connects the thigh and shank of the human body [1,2]. In daily activities such as normal walking or running, the knee can tolerate moderate stress without significant injury. But the knee lacks support to withstand undue rotational forces and other types of physical trauma [3,4]. Knee degenerative arthritis is a type of mechanical abnormality due to articular cartilage deterioration, which could be caused by overloaded knee motion or accidental trauma to the knee. At present, arthroscopy and medical imaging are most commonly used in the diagnostic procedure of knee joint arthritis and other disorders. The arthroscopic examinations are most frequently used to inspect the inflammation, tears of meniscus, chondromalacia (wearing or injury of cartilage cushion), and anterior cruciate ligament tears [2]. In a knee arthroscopic examination, an orthopaedic surgeon makes a small incision in the patient's skin and then inserts pencil-sized instruments that contain a small lens and lighting system to magnify and illuminate the interior structures of the joint. It may increase the surgical success rate due to less trauma to the connective tissue, and could also save recovery time. But it is still a semi-invasive surgical procedure that cannot be frequently applied in the routine examinations, because the same incision that undergos repeated surgical invasions is susceptible to bacterial infection. Computer tomography and traditional X-rays scanning approaches use ionizing radiation to detect the bone conditions. The soft tissues and articular cartilage are usually blurred in the X-ray images because their density is relatively lower than that of bones. Magnetic resonance imaging may distinguish the articular cartilage and synovial fluid in the knee joint by adjusting the image contrast resolution [5]. Medical imaging techniques can display anatomical morphology of the knee joint, but the imaging protocol cannot support functional detection of the knee joint conditions during leg movements, because the subject has to lay down throughout the imaging scanning procedure.

* Corresponding author. Tel.: +86 592 2194658; fax: +86 592 5095058.
E-mail addresses: y.wu@ieee.org, cloudswu@gmail.com (Y. Wu).

http://dx.doi.org/10.1016/j.medengphy.2014.07.008
1350-4533/

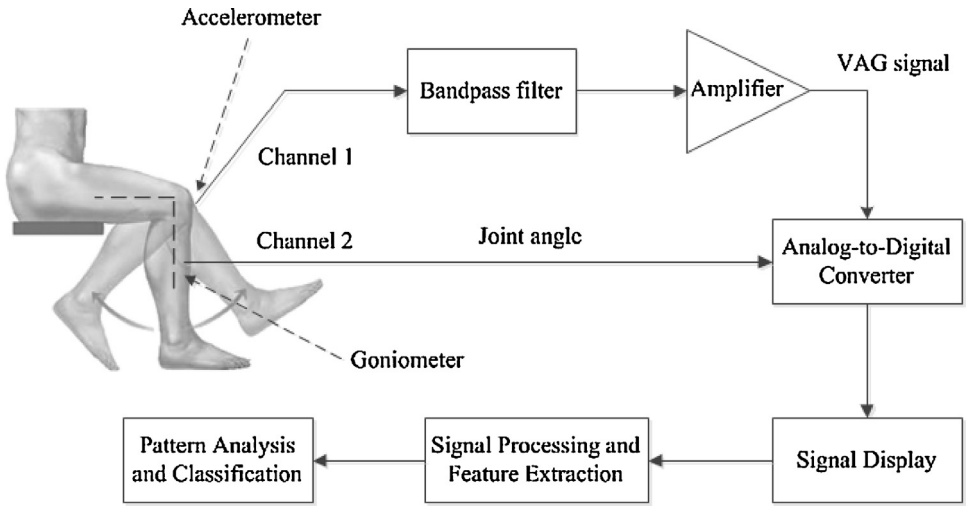

Fig. 1. Illustration of vibration arthrometry procedures to record and analyze the knee joint vibroarthrographic (VAG) signals.

Vibration arthrometry is an alternative noninvasive technology to detect the knee joint pathology [6–9]. The vibration arthrometry records the knee joint vibroarthrographic (VAG) signal by using accelerometers or electro-stethoscope sensors on the knee [10–13]. Fig. 1 shows the vibration arthrometry work flow which commonly contains the procedures of signal conditioning, signal display, signal processing, feature extraction, and patter classification. The VAG signals of patients with knee joint disorders usually exhibit different characteristics from those of healthy adults. For healthy adults, their articular surfaces in the knee are smooth and slippery without any cartilage friction or collision during knee flexion or extension motions [1]. However, the vibrations generated due to friction between the degenerative articular cartilages are expected to present anomalous patterns in the amplitude and frequency scales [3,15,14]. Computer-assisted analysis of knee joint VAG signals is very useful for feature representation in the time-frequency scale [15,16]. Based on the distinct features extracted [13,17–19], computational algorithms can effectively help screening and monitoring of articular cartilage disorders at an early stage, so that the frequency of arthroscopic examinations could be dwindled [10,20–22]. The recent experiments of Tanaka and Hoshiyama also demonstrated that the VAG signals are useful for identification of functional knee joint pathology when the patients perform standing-up and sitting-down movements [14].

The major contributions of the present study are summarized as follows. First, two distinct features were extracted to characterize the fluctuation dynamics of the knee joint VAG signals. The detrended fluctuation analysis (DFA) method was applied to compute the statistical self-affinity properties of the signals over the time scale. The normal VAG signal is supposed to be with less self-affinity because a healthy knee commonly produces little articular surface friction in the course of knee flexion and extension motions. On the other hand, the pathological VAG signal should contain more correlated components generated by the complex physiological process due to knee pathology. It is hypothesized that the normal and pathological VAG signals possess significantly different self-affinity properties in terms of fractal scaling index. The averaged envelope amplitude was calculated to measure the degree of temporal signal varying on average. It is hypothesized that the averaged envelope amplitude parameter of the VAG signal associated with pathological conditions should be larger than that of the signal recorded from a healthy adult. Second, the kernel density modeling method was employed to estimate the distributions of the signal patterns in the bivariate feature space. Finally, the maximal posterior probability decision criterion and the support vector machine were used to perform the binary classifications for the VAG signals of healthy subjects and patients with knee joint disorders.

2. Materials and methods

2.1. Dataset preparation

The data set used in our experiments was provided by Rangayyan's research group at University of Calgary. The knee joint VAG signals were recorded from 75 subjects, who were categorized into the normal and pathological groups [10]. The normal group contained 47 healthy adults, whose knees were confirmed by physical examinations and medical historical records. The pathological group included 28 patients with knee joint disorders, who had the symptoms of patellar and tibial chondromalacia, cruciate ligament injury, or tears of meniscus. The pathological condition of the knee joint was confirmed in the independent arthroscopic examination for each patient. The subjects provide their written informed consent to participate in the data acquisition experiments. The experiment protocol and subject consent documents were approved by the Conjoint Health Research Ethics Board of the University of Calgary. The signal processing and data analysis methodology documents were reviewed by the Ethics Committee of Xiamen University.

According to the data acquisition protocol [10], each subject was requested to sit on a rigid chair and voluntarily swing one shank over the angle range from 135◦ (approximately full flexion) to 0◦ (full extension), and then back to 135◦ in 4 s. The knee joint VAG time series was recorded with a miniature accelerometer attached at the middle-patella position using two-sided adhesive tape. The raw signals were digitized with the sampling rate of 2 kHz and the sample resolution of 12 bit, which allowed to detect the high-frequency physiological click events when the subject performed the knee extension and flexion motions. The artifact of baseline wander was removed by a 20th-order cascade moving average filter [23].

2.2. Extraction of signal fluctuation features

2.2.1. Fractal scaling index

Fractal scaling index (denoted as α) is a type of parameter that describes the subtle fluctuations associated with the intrinsic correlations of signal dynamics. The fractal scaling index can be computed with the detrended fluctuation analysis (DFA) algorithm, which is commonly used to study the statistical self-affinity of the

signal tested [24,25]. The DFA algorithm is very useful for detecting the nonstationary time series with long-range correlations [26].

For an N-length VAG signal $s(n)$ with the mean value of $\bar{s}$, the integrated time series $y(i)$ is defined by $y(i) = \sum_{n=1}^{i} [s(n) - \bar{s}]$. Then, the integrated time series $y(i)$ is divided into several segment windows of equal size k, with a least-squares line called the local linear trend to fit the window samples [27] The local detrended fluctuation is then computed by subtracting the local linear trend $y_k(i)$ from the integrated time series $y(i)$ in each segment window. The averaged fluctuation $F(k)$ is derived from the root-mean-square of the local detrended fluctuations as

$$F(k) = \left[\frac{1}{N} \sum_{i=1}^{N} [y(i) - y_k(i)]^2 \right]^{1/2}. \quad (1)$$

The averaged fluctuation computation is repeated over all time scales for each VAG signal that contains 8000 samples in length, with the window sizes in the range [4, 8, 16, 31, 63, 125, 250, 500, 1000, 2000, 4000, 8000]. In practice, the function relating the averaged fluctuation $F(k)$ to the window size k is commonly represented on a double logarithm graph [25]. The fractal scaling index, α, is computed as the slope of the linear relationship between $\log F(k)$ and $\log k$, which is also known as a power law $F(k) \sim k^{\alpha}$. The integrated and detrended time series with persistent long-range power-law correlations possess a fractal scaling index value $0.5 < \alpha < 1$. On the other hand, a result of $0 < \alpha < 0.5$ indicates an anti-correlated property of the time series [28].

2.2.2. Averaged envelope amplitude

The fluctuations in a rapidly shifting signal can also be described by the envelope parameter. The envelope sketches the appearance of the signal in the time domain, that is, the envelope represents the boundary of the signal samples in amplitude.

For the VAG signal associated with pathological conditions, the time series commonly vary with large amplitudes due to friction on the degenerative articular surfaces in the knee joint. In the present study, each VAG signal was first split into the equal-length segments with the time slots of 0.01 s (window length of 20 samples). The local extremes (the largest positive peak and the lowest negative peak) were then estimated in each time slot. Next, the upper and lower envelopes were outlined with the linear interpolations between the successive local extremes. The envelope amplitude was used to measure the boundary between the upper and lower envelopes of each VAG signal, and we computed the averaged envelope amplitude, denoted as δ, to characterize the degree of signal fluctuations on average.

2.2.3. Statistical test

In the present study, two-sample Kolmogorov–Smirnov (K–S) test [29] was applied to test for statistical significance of the extracted features between the normal and pathological signal groups. The two-sample K–S test is a type of nonparametric approach that makes no assumptions about the underlying distribution of the data being compared. The level of statistical significance was set to be $p \leq 0.01$.

2.3. Kernel density modeling in feature space

The VAG signal of a patient with knee joint disorders sometimes exhibits the complex morphological patterns generated by the physiological process associated with pathological conditions. It is therefore quite difficult to estimate the feature densities using some standard distribution models. The kernel density modeling method is able to establish the unimodal or multimodal density functions in multivariate feature space [30], which makes it very suited for the feature density estimations of the normal and pathological VAG signal groups.

With the features of fractal scaling index and averaged envelope amplitude, the VAG signal can be represented with a feature vector $\mathbf{x} = [x_\alpha, x_\delta]^T$. Let ω be the class label of a VAG signal group, with ω_N and ω_P denoting the normal and pathological groups, respectively. The class-conditional probability density can be estimated with the kernel functions based on the M signal instances in a particular group [30,31], i.e.,

$$p(\mathbf{x}|\omega) = \frac{1}{M} \sum_{m=1}^{M} g(\mathbf{x}^m|\omega). \quad (2)$$

In the present study, we used the bivariate Gaussian window to construct the kernel function as

$$g(\mathbf{x}|\omega) = \frac{1}{2\pi \left|\sum\right|^{1/2}} \exp\left[-\frac{1}{2} (\mathbf{x} - \boldsymbol{\mu}^m)^T \sum^{-1} (\mathbf{x} - \boldsymbol{\mu}^m) \right], \quad (3)$$

the center of which locates at $\boldsymbol{\mu}^m = \left[\mu_\alpha^m, \mu_\delta^m\right]^T$, in accordance with the feature vector of the m-th VAG signal associated with the group ω. The spread width of the Gaussian kernel is determined by the symmetric and positive definite covariance matrix $\boldsymbol{\Sigma} = \eta \begin{bmatrix} \sigma_\alpha^2 & \rho\sigma_\alpha\sigma_\delta \\ \rho\sigma_\alpha\sigma_\delta & \sigma_\delta^2 \end{bmatrix}$, in which $\rho = 0.32$ denotes the correlation coefficient between the fractal scaling index and averaged envelope amplitude, $\eta = 0.08$ represents the scaling factor that controls the spread area of the Gaussian kernel in the two-dimensional feature space, and $\sigma_\alpha = 0.11$ and $\sigma_\delta = 0.19$ are the standard deviations of x_α and x_δ, respectively. The covariance matrix $\boldsymbol{\Sigma} = \begin{bmatrix} 0.0009 & 0.0005 \\ 0.0005 & 0.0028 \end{bmatrix}$ was set to be the same for both of the normal and pathological VAG signal groups.

2.4. Signal classification

2.4.1. Bayesian decision rule

Given a VAG signal, the posterior probability $P(\omega|\mathbf{x})$ presents the possibility of the signal belonging to the group ω, conditioned on the observation of feature vector $\mathbf{x}$. The posterior probability $P(\omega|\mathbf{x})$ can be computed from $p(\mathbf{x}|\omega)$ by Bayes' formula [32]:

$$P(\omega|\mathbf{x}) = \frac{p(\mathbf{x}|\omega)P(\omega)}{p(\mathbf{x})}, \quad (4)$$

where the prior probability $P(\omega)$ indicates the possible occurrence of a VAG signal group. The evidence factor $p(\mathbf{x})$ is the sum of the product between the class-conditional probability density and prior probability for the normal and pathological signal groups, i.e.,

$$p(\mathbf{x}) = p(\mathbf{x}|\omega_N)P(\omega_N) + p(\mathbf{x}|\omega_P)P(\omega_P). \quad (5)$$

In this case, the posterior probability $P(\omega|\mathbf{x})$ can also be expressed as:

$$P(\omega|\mathbf{x}) = \frac{p(\mathbf{x}|\omega)P(\omega)}{p(\mathbf{x}|\omega_N)P(\omega_N) + p(\mathbf{x}|\omega_P)P(\omega_P)}. \quad (6)$$

The Baysian decision is then made as $\arg\max_{\omega} P(\omega|\mathbf{x})$, by assigning the class label ω to the signal $\mathbf{x}$ with respect to the maximum posterior probability $P(\omega|\mathbf{x})$ between the normal and pathological groups.

2.4.2. Least-squares support vector machine

In addition to the Bayesian decision rule, the least-squares support vector machine (LS-SVM) was also employed to perform the signal classifications. The support vector machine (SVM) proposed

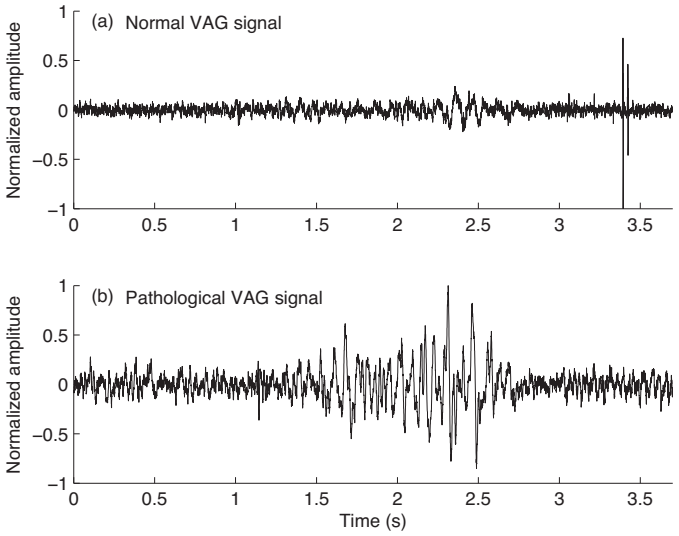

Fig. 2. Examples of knee joint vibroarthrographic (VAG) signals recorded from (a) a healthy female subject of 32 years old, and (b) a male patient of 35 years old suffering from tear of lateral meniscus. The amplitude range of the normal VAG signal is relatively small except for those samples associated with the physiological click events. A number of large oscillations occur in the pathological VAG signal due to the tear of lateral meniscus.

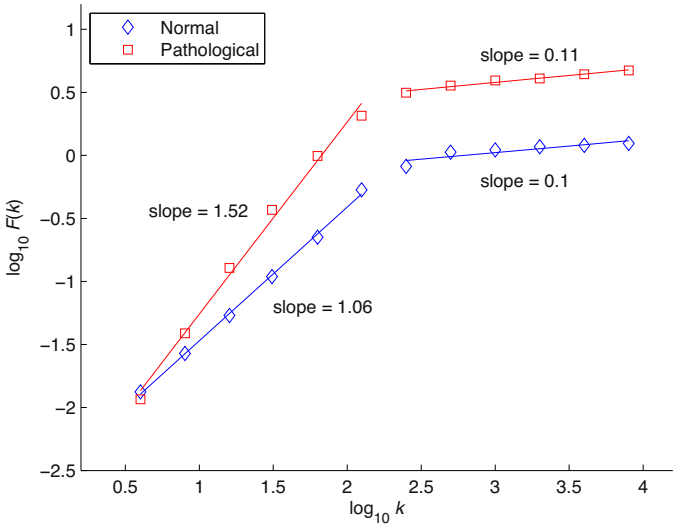

Fig. 3. Plots of $\log_{10}F(k)$ versus $\log_{10}k$ for the normal (32-year-old female subject) and pathological (35-year-old male subject with lateral meniscal tear) knee joint VAG signals shown in Fig. 2. The squares and diamonds indicate the averaged fluctuation computed from the integrated time series in different time scales for the healthy female subject and the patient with lateral meniscal tear, respectively.

by Cortes and Vapnik is a supervised learning paradigm that follows the structural risk minimization principle [33]. Nonlinear inner-product kernels enable the SVM to perform nonlinear classifications by mapping the inputs into high-dimensional spaces. By tuning the model parameters during the training process, the SVM selects some informative patterns as the support vectors to construct a hyperplane as the decision surface that maximizes the margin of separation between different classes [34]. The LS-SVM is a modification version of the classical SVM, with an improvement of moderate complexity. The optimization of the LS-SVM is obtained by the minimization of a regularized least-squares cost function with equality constraints under the Karush–Kuhn–Tucker condition [35], which is different from the learning of the classical SVM with a constrained quadratic programming solution [34]. The methodology details of the classical SVM and the LS-SVM have been well described in the literature [33–35]. In the present study, the LS-SVM works with the polynomial kernels given by $\varphi(\mathbf{x}_j, \mathbf{x}_l) = (\mathbf{x}_j^T\mathbf{x}_l + t)^d$, where d denotes the degree of the polynomial, and t is the intercept. The reason to choose the polynomial kernels for the LS-SVM was that the other types of nonlinear inner-product kernels would bring several isolated decision islands with one signal each, which makes some difficulties of pathological inference in the feature space. In our experiments, the optimal degree $d = 3$ and intercept $t = 1$ parameters of the polynomial kernels were set to help the LS-SVM produce the highest accuracy in the VAG signal classification task.

3. Results and discussion

A pair examples of knee joint VAG signals recorded from a healthy subject (female, aged 32 years) and a patient (male, aged 35 years) with lateral meniscal tear are illustrated in Fig. 2. The healthy subject exercises more than 3 times per week, which is regarded with a high activity level. Besides two physiological clicks observed from 3.39–3.42 s in Fig. 2(a), her VAG signal presents very slight morphological variations from 2.28–2.52 s, but the knee joint is still under the healthy condition, as tested in the physical examinations with medical imaging modality. For the age-matched patient with lateral meniscal tear who only exercises once per week or less, the corresponding VAG signal exhibits larger fluctuations in comparison with the normal signal, especially in the duration of 1.53–2.72 s as displayed in Fig. 2(b).

Fig. 3 plots the averaged fluctuation $F(k)$ with respect to the scaling window size k, both of which are expressed in the common logarithm (base 10) sense, for the normal and pathological VAG signals depicted in Fig. 2. It is noted that, for the long-range time scales ($250 \le k \le 8000$), both of the integrated and detrended time series computed from the normal and pathological VAG signals show the anti-correlation properties ($\alpha \approx 0.1$). However, for the short-range time scales ($4 \le k \le 125$), the integrated time series $F(k)$ of the normal VAG signal is closer to Brown noise (the integration of white noise [25]), and $F(k)$ associated with the pathological signal presents power-law correlations (i.e., $1/f$ noise). It is intuitively observed that the window size k is better to be lower than the crossover value of 250 for the fractal analysis of VAG signals, because the slope of $\log_{10}F(k)$ to $\log_{10}k$ is not much different between the normal and pathological signals when $\log_{10}k$ is larger than 2.5. In the present work, we computed the fractal scaling index (α) for the total 75 VAG signals over all time scales. The normal signal group tend to possess an averaged fractal scaling index of 0.533 (standard deviation, SD: 0.096), the bar graph of which is shown in Fig. 5. On the other hand, the pathological signal group possesses a significantly different ($p = 0.0001$) distribution of the fractal scaling index feature (mean ± SD: 0.635 ± 0.092).

In addition to fractal scaling index, the averaged envelope amplitude feature also manifests the fluctuation characteristics of the VAG signals. For the normal and pathological VAG signals shown in Fig. 2, the upper (blue line) and lower (red line) envelopes of the VAG signal segments are outlined in Fig. 4. The signal fluctuations are measured in terms of the difference between the upper and lower envelopes (i.e., the envelope amplitude). It can be observed that the pathological signal segment zoomed-in from 1.4–2.4 sec exhibits apparently higher degree of fluctuations than the normal signal segment of equal-length (zoomed-in from 1–2 s). The averaged envelope amplitude feature indicates the general fluctuation degree of a VAG signal. The results shows that the averaged envelope amplitude of the pathological signals (0.434 ± 0.154) is significantly increased ($p = 0.0001$), in comparison with that of the normal signals (0.267 ± 0.179).

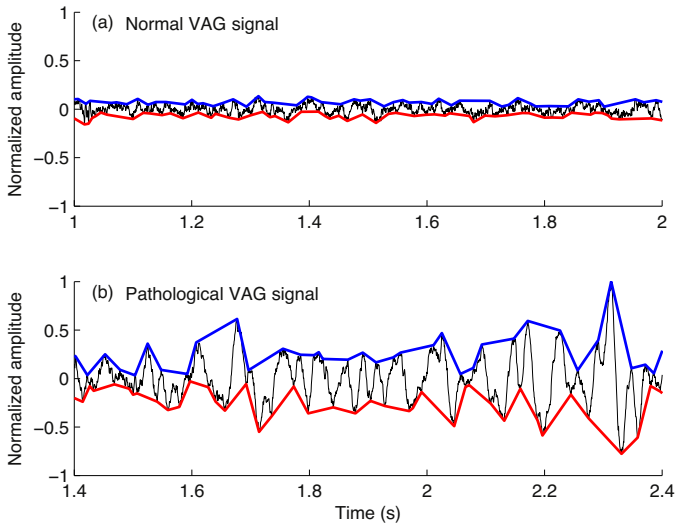

Fig. 4. Illustrations of the upper and lower envelopes estimated from the knee joint vibroarthrographic signals shown in Fig. 2.

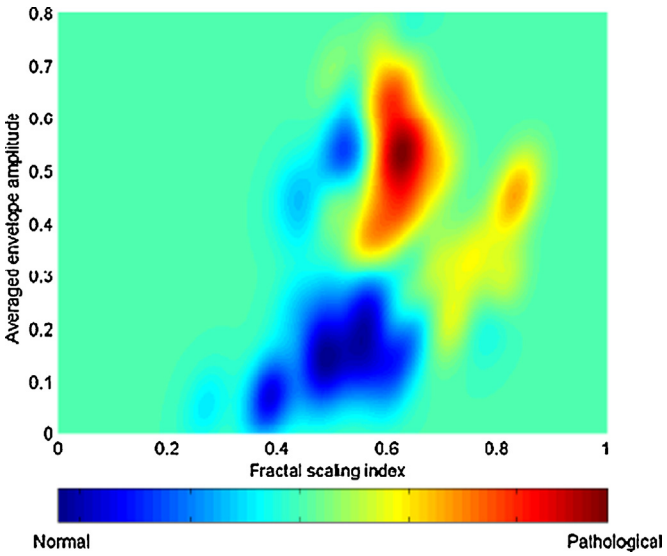

Fig. 6. Distributions of the bivariate features for the normal and abnormal knee joint vibroarthrographic signals. The distribution of the normal signals is shown with the cold color map (blue representing the highest density), whereas the distribution of the abnormal signals is illustrated with the hot color map (red representing the highest density). (For interpretation of the references to color in this figure legend, the reader is referred to the web version of this article.)

Fig. 5 provides the bar graphics of the fractal scaling index and averaged envelope amplitude results for the normal and pathological groups. It is noted that the difference of averaged envelope amplitude is somewhat larger than the fractal scaling index difference, between the normal and pathological signal groups.

The feature distributions of the normal and pathological signal groups are visible in Fig. 6. Both of the two VAG signal groups possess multimodal densities in the bivariate feature space. Majority of the normal signals aggregate in the area with the fractal scaling index lower than 0.65 and the averaged envelope amplitude lower than 0.3. On the other hand, the pathological signals converge with two large clusters in the top right corner. Instead of just plotting the scatters in the feature space, the kernel density modeling method can describe the aggregation or divergence conditions of signal patterns with their estimated densities. The contours shown in Fig. 6 indicate the visible transition of signal patterns from the healthy group to the pathological group.

Fig. 7 plots the scatter patterns of the normal signals (marked as circles) and pathological signals (marked as triangles). There are a few pathological signal patterns mingled with the pattern clusters of normal signals, which makes some difficulties for a linear discrimination. The LS-SVM with polynomial kernels and the Bayesian decision rule provides two different nonlinear discriminant boundaries. The decision boundary of the LS-SVM is a smooth parabola that can successfully distinguish 62 (44 normal and 18 pathological) signals, with an overall accurate rate of 82.67% for the VAG signal classification. The Bayesian decision rule, on the other hand, better separates the bulge signal scatters. Table 1 lists the classification performance results in our experiments. The overall accurate rate of the Bayesian decision rule reaches 88% which is slightly higher than that of the LS-SVM. According to Table 1, the Bayesian decision rule produces a sensitivity (SEN) of 71.43%, specificity (SPE) of 97.87%, and positive precision rate (PPR) of 95.24%, which are consistently better than those obtained by the LS-SVM (SEN: 64.29%, SPE: 93.62%, PPR: 85.71%), and the results of the k-nearest neighbor classifier ($k = 5$) with input features of FF and VMS (OCA: 80%, SEN: 71.43%, SPE: 85.11%) [38]. The better results of the Bayesian decision rule owing to correct classifications of 4 more (2 normal and 2 pathological) signals among the bulge scatters shown in Fig. 7.

The Bayesian decision rule also provides a larger area value A_z of 0.957 under the receiver operating characteristic curve than the LS-SVM (A_z: 0.867). Table 2 summarizes the diagnostic results reported in the previous related studies [13,17,36,22,21,37]. The new fluctuation features (fractal scaling index and averaged

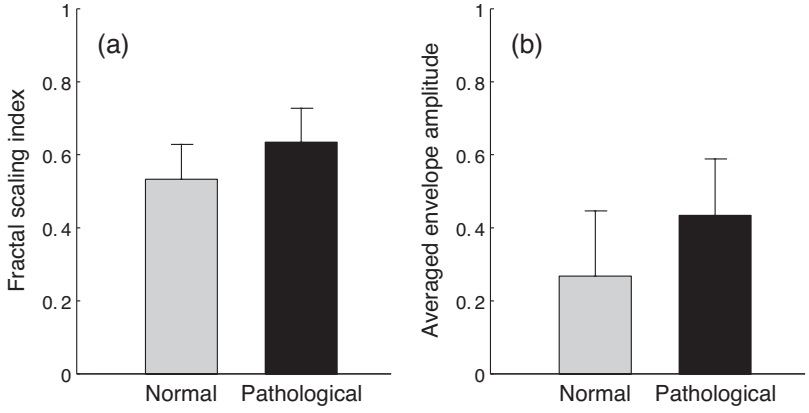

Fig. 5. Bar graphs of the fractal scaling index (normal group: 0.533 ± 0.096, pathological group: 0.635 ± 0.092) and averaged envelope amplitude (normal group: 0.267 ± 0.179, pathological group: 0.434 ± 0.154) computed from the vibroarthrographic signals.

Table 1
The diagnostic performance of the least-squares support vector machine (LS-SVM) and the Bayesian decision rule (BDR) for classification of knee joint vibroarthrographic signals.

	AP	AN	TP	FP	TN	FN	SEN(%)	SPE(%)	PPR(%)	OCA(%)	A_z
LS-SVM	28	47	18	3	44	10	64.29	93.62	85.71	82.67	0.867
BDR	28	47	20	1	46	8	71.43	97.87	95.24	88	0.957

The signal classifications were evaluated by the diagnostic parameters of AP (actual positive), AN (actual negative), TP (true positive), FN (false negative), TN (true negative), FP (false positive), sensitivity: SEN = TP/(TP + FN), specificity: SPE = TN/(TN + FP), positive precision rate: PPR = TP/(TP + FP), overall classification accuracy: OCA = (TP + TN)/(TP + FN + TN + FP), and A_z (area under the receiver operating characteristic curve).

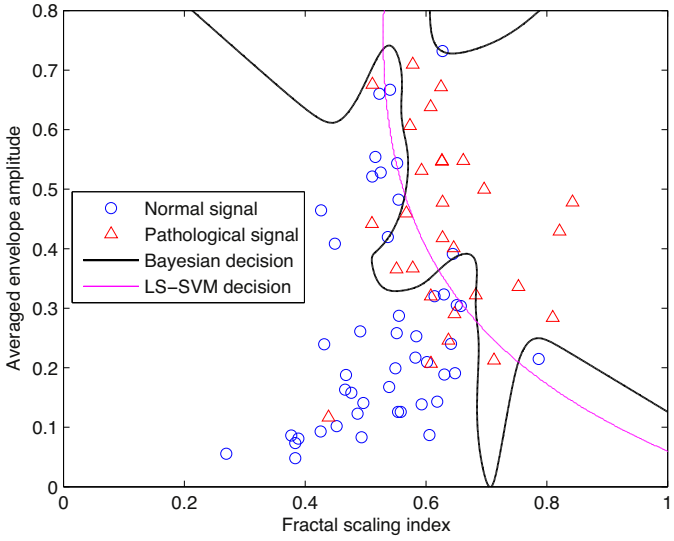

Fig. 7. Decision boundaries provided by the least-squares support vector machine (LS-SVM) with polynomial kernels and the Bayesian decision rule.

envelope amplitude) developed in the present study are able to help the Bayesian decision rule achieve better classification performance than the maximal posterior probability decision criterion (accuracy: 86.67%, A_z: 0.9096, with FF and VMS features) [22], and the multiple classifier system based on the recurrent neural network (accuracy: 80.9%, A_z: 0.9484, with form factor, skewness, kurtosis, entropy, turns count, and variance of mean-square values features) [21]. The diagnostic results of the Bayesian decision rule are also comparable with the results of the radial basis function network (highest A_z: 0.961, with form factor, difference between the Kullback-Leibler distance, turns count, fractal dimensions, and skewness features [19]), of the strict 2-surface proximal classifier (A_z: 0.95, with the form factor, skewness, kurtosis, entropy features) [36], and of the dynamic weighted classifier fusion system (A_z: 0.9515, with number of wavelet matching pursuit decomposition and turns count with the fixed threshold features [37]).

Table 2
The diagnostic results of different classification methods with the knee joint vibroarthrographic signal features developed in the previous studies [13,17–19,21,22,36,37].

Features	Methods	A_z
FF, S, K, H	Radial basis function network	0.82
FF, S, K, H	Strict 2-surface proximal classifier	0.95
TC, VMS	Radial basis function network	0.9174
dKLD, K, H, μ, σ	Radial basis function network	0.8322
FF, dKLD, TC, FD, S	Radial basis function network	0.961
FF, VMS	Maximal posterior probability decision criterion	0.9096
FF, S, K, H, TC, VMS	Multiple classifier system	0.9484
Natom, TCFT	Dynamic weighted classifier fusion system	0.9515

FF: form factor, S: skewness, K: Kurtosis, H: entropy, TC: turns count, VMS: variance of mean-squared values, dKLD: difference between the Kullback–Leibler distances of the normal and abnormal signal probability density functions, μ: mean, σ: standard deviation, FD: fractal dimensions, Natom: number of wavelet matching pursuit decomposition, TCFT: turns count with the fixed threshold.

The fractal scaling index parameter measures the inherent self-similarity property of VAG signals. Our experimental results show that the pathological signals usually contain more components with long-range power-law correlations than the normal signals. The averaged envelope amplitude parameter describes the level of signal oscillations in amplitude. The results indicate that a pathological VAG signal is more likely to possess a larger value of averaged envelope amplitude. These new parameters can help effective screening of VAG signals in clinical practice. In addition, the VAG time series with the envelop boundaries attached (see Fig. 4) can provide a better visual representation of signal fluctuations for fast point-of-care diagnostics.

4. Conclusion

Distinct features of VAG signals developed with signal processing techniques are useful for analysis of knee joint osteoarthropathy, chondromalacia, and tears of meniscus [14,37,39]. Computational methods can effectively represent features in high-dimensional space for a better classification of VAG signals. The present study extracted two new features, i.e., the fractal scaling index and averaged envelope amplitude, which can be used to characterize the fluctuation degree of VAG signals. The kernel density modeling method can evidently represent the distributions of the normal and pathological signal groups in the bivariate feature space. The Bayesian decision rule utilized the feature density information to distinguish the pathological VAG signals from the normal signals, with high diagnostic accuracy. The encouraging experiment results demonstrated the effectiveness of the computational methods for classification of VAG signals. Future work could focus on the development of novel mathematical models and algorithms [40], for assessment of articular cartilage degeneration and diagnosis of particular knee joint disorders such as chondromalacia and tears of meniscus.

Ethical approval

The experiment protocol and subject consent documents were approved by the Conjoint Health Research Ethics Board of the University of Calgary. The signal processing and data analysis methodology documents were reviewed by the Ethics Committee of Xiamen University.

Acknowledgements

The authors would like to thank Rangaraj M. Rangayyan, Cyril B. Frank, and Gordon D. Bell, for the work of data acquisition. Financial supports from the National Natural Science Foundation of China (no.: 81101115, 31200769, 61370010, 81272168) and the Fundamental Research Funds for the Central Universities of China (no.: 2010121061) are gratefully acknowledged. Yunfeng Wu and

Meihong Wu were also supported by the Program for New Century Excellent Talents in Fujian Province University.

Conflict of interest

There is no conflict of interest.

References

[1] Wu Y, Krishnan S, Rangayyan RM. Computer-aided diagnosis of knee-joint disorders via vibroarthrographic signal analysis: a review. Crit Rev Biomed Eng 2010;38(2):201–24.
[2] Wu Y. Knee joint vibroarthrographic signal processing and analysis. Heidelberg: Springer-Verlag; 2014.
[3] Frank CB, Rangayyan RM, Bell GD. Analysis of knee sound signals for non-invasive diagnosis of cartilage pathology. IEEE Eng Med Biol Mag 1990;9(1):65–8.
[4] Vigorita VJ. Orthopaedic pathology. Philadelphia, PA: Lippincott Williams and Wilkins; 1999.
[5] Manaster BJ, Crim J, Rosenberg ZS. Diagnostic and surgical imaging anatomy: knee ankle foot. Philadelphia, PA: Lippincott Williams and Wilkins; 2007.
[6] McCoy GF, McCrea JD, Beverland DE, Kernohan WG, Mollan RAB. Vibration arthrography as a diagnostic aid in diseases of the knee: a preliminary report. J Bone Joint Surg Br 1987;69-B(2):288–93.
[7] Lee JH, Jiang CC, Yuan TT. Vibration arthrometry in patients with knee joint disorders. IEEE Trans Biomed Eng 2000;47(8):1131–3.
[8] Jiang CC, Lee JH, Yuan TT. Vibration arthrometry in the patients with failed total knee replacement. IEEE Trans Biomed Eng 2000;47(2):218–27.
[9] Abbott SC, Cole MD. Vibration arthrometry: a critical review. Crit Rev Biomed Eng 2013;41(3):223–42.
[10] Rangayyan RM, Krishnan S, Bell GD, Frank CB, Ladly KO. Parametric representation and screening of knee joint vibroarthrographic signals. IEEE Trans Biomed Eng 1997;44(11):1068–74.
[11] Krishnan S, Rangayyan RM, Bell GD, Frank CB. Adaptive time-frequency analysis of knee joint vibroarthrographic signals for noninvasive screening of articular cartilage pathology. IEEE Trans Biomed Eng 2000;47(6):773–83.
[12] Krishnan S, Rangayyan RM, Bell GD, Frank CB. Auditory display of knee-joint vibration signals. J Acoust Soc Am 2001;110(6):3292–304.
[13] Rangayyan RM, Wu YF. Screening of knee-joint vibroarthrographic signals using statistical parameters and radial basis functions. Med Biol Eng Comput 2008;46(3):223–32.
[14] Tanaka N, Hoshiyama M. Vibroarthrography in patients with knee arthropathy. J Back Musculoskelet Rehabil 2012;25(2):117–22.
[15] Kim KS, Seo JH, Kang JU, Song CG. An enhanced algorithm for knee joint sound classification using feature extraction based on time-frequency analysis. Comput Meth Programs Biomed 2009;94(2):198–206.
[16] Krishnan S, Rangayyan RM. Automatic de-noising of knee-joint vibration signals using adaptive time-frequency representations. Med Biol Eng Comput 2000;38(8):2–8.
[17] Rangayyan RM, Wu Y. Analysis of vibroarthrographic signals with features related to signal variability and radial-basis functions. Ann Biomed Eng 2009;37(1):156–63.
[18] Rangayyan RM, Wu Y. Screening of knee-joint vibroarthrographic signals using probability density functions estimated with Parzen windows. Biomed Signal Process Control 2010;5(1):53–8.
[19] Rangayyan RM, Oloumi F, Wu Y, Cai S. Fractal analysis of knee-joint vibroarthrographic signals via power spectral analysis. Biomed Signal Process Control 2013;8(1):26–9.
[20] Umapathy K, Krishnan S. Modified local discriminant bases algorithm and its application in analysis of human knee joint vibration signals. IEEE Trans Biomed Eng 2006;53(3):517–23.
[21] Wu Y, Krishnan S. Combining least-squares support vector machines for classification of biomedical signals: a case study with knee-joint vibroarthrographic signals. J Exp Theor Artif Intell 2011;23(1):63–77.
[22] Wu Y, Cai S, Yang S, Zheng F, Xiang N. Classification of knee joint vibration signals using bivariate feature distribution estimation and maximal posterior probability decision criterion. Entropy 2013;15(4):1375–87.
[23] Cai S, Wu Y, Xiang N, Zhong ZT, He J, Shi L, Xu F. Detrending knee joint vibration signals with a cascade moving average filter. In: Proceedings of the 34th annual international conference of IEEE engineering in medicine and biology society. Piscataway, NJ: IEEE; 2012. p. 4357–60.
[24] Peng CK, Buldyrev SV, Goldberger AL, Havlin S, Sciortino F, Simons M, Stanley HE. Long-range correlations in nucleotide sequences. Nature 1992;356:168–70.
[25] Peng CK, Havlin S, Stanley HE, Goldberger AL. Quantification of scaling exponents and crossover phenomena in nonstationary heartbeat time series. Chaos 1995;5(1):82–7.
[26] Bak P, Tang C, Wiesenfeld K. Self-organized criticality: an explanation of the 1/f noise. Phys Rev Lett 1987;59:381–4.
[27] Wu Y, Yang S, Zheng F, Cai S, Lu M, Wu M. Removal of artifacts in knee joint vibroarthrographic signals using ensemble empirical mode decomposition and detrended fluctuation analysis. Physiol Meas 2014;35(3):429–39.
[28] Kantelhardt JW, Koscielny-Bunde E, Rego HH, Havlin S, Bunde A. Detecting long-range correlations with detrended fluctuation analysis. Physica A 2001;295(3):441–54.
[29] Casella G, Berger RL. Statistical inference. 2nd ed. Pacific Grove, CA: Duxbury Press; 2001.
[30] Parzen E. On estimation of a probability density function and mode. Ann Math Stat 1962;33(3):1065–76.
[31] Yang S, Zheng F, Luo X, Cai S, Wu Y, Liu K, Wu M, Chen J, Krishnan S. Effective dysphonia detection using feature dimension reduction and kernel density estimation for patients with Parkinson's disease. PLoS ONE 2014;9(2):e88825.
[32] Duda RO, Hart PE, Stork DG. Pattern classification. 2nd ed. New York, NY: Wiley; 2001.
[33] Cortes C, Vapnik VN. Support-vector networks. Mach Learn 1995;20(3):273–97.
[34] Vapnik VN. Statistical learning theory. New York, NY: Wiley; 1998.
[35] Suykens JAK, Van Gestel T, De Brabanter J, De Moor B, Vandewalle J. Least squares support vector machines. Singapore: World Scientific Publishing; 2002.
[36] Mu T, Nandi AK, Rangayyan RM. Screening of knee-joint vibroarthrographic signals using the strict 2-surface proximal classifier and genetic algorithm. Comput Biol Med 2008;38(10):1103–11.
[37] Cai S, Yang S, Zheng F, Lu M, Wu Y, Krishnan S. Knee joint vibration signal analysis with matching pursuit decomposition and dynamic weighted classifier fusion. Comput Math Method Med 2013;2013:904267.
[38] Liu K, Luo X, Zheng F, Yang S, Cai S, Wu Y. Classification of knee joint vibroarthrographic signals using k-nearest neighbor algorithm. In: Proceedings of the 27th Canadian conference on electrical and computer engineering. Piscataway, NJ: IEEE; 2014. p. 150–3.
[39] Wu Y, Cai S, Xu F, Shi L, Krishnan S. Chondromalacia patellae detection by analysis of intrinsic mode functions in knee joint vibration signals. In: IFMBE Proceedings of 2012 world congress on medical physics and biomedical engineering. Heidelberg: Springer; 2013. p. 493–6.
[40] Wu Y, Luo X, Zheng F, Yang S, Cai S, Ng SC. Adaptive linear and normalized combination of radial basis function networks for function approximation and regression. Math Probl Eng 2014;2014:913897.